Subthreshold outward currents enhance temporal integration in auditory neurons

Gytis Svirskis[1,2], **Ramana Dodla**[1], and **John Rinzel**[1,3]

[1]Center for Neural Science, New York University, New York, NY 10003, USA

[2]Laboratory of Neurophysiology, Biomedical Research Institute, Kaunas Medical University, 3000 Kaunas, Lithuania

[3]Courant Institute of Mathematical Sciences, New York University, New York, NY 10012, USA

Abstract

Many auditory neurons possess low-threshold potassium currents (I_{KLT}) that enhance their responsiveness to rapid and coincident inputs. We present recordings from gerbil medial superior olivary (MSO) neurons in vitro and modeling results that illustrate how I_{KLT} improves the detection of brief signals, of weak signals in noise, and of the coincidence of signals (as needed for sound localization). We quantify the enhancing effect of I_{KLT} on temporal processing with several measures: signal-to-noise ratio (SNR), reverse correlation or spike-triggered averaging of input currents, and inter-aural time difference (ITD) tuning curves. To characterize how I_{KLT}, which activates below spike threshold, influences a neuron's voltage rise toward threshold, i.e., how it filters the inputs, we focus first on the response to weak and noisy signals. Cells and models were stimulated with a computer-generated steady barrage of random inputs, mimicking weak synaptic conductance transients (the "noise"), together with a larger but still subthreshold postsynaptic conductance, EPSG (the "signal"). Reduction of I_{KLT} decreased the SNR, mainly due to an increase in spontaneous firing (more "false positive"). The spike-triggered reverse correlation indicated that I_{KLT} shortened the integration time for spike generation. I_{KLT} also heightened the model's timing selectivity for coincidence detection of simulated binaural inputs. Further, ITD tuning is shifted in favor of a slope code rather than a place code by precise and rapid inhibition onto MSO cells (Brand et al. 2002). In several ways, low-threshold outward currents are seen to shape integration of weak and strong signals in auditory neurons.

1 Introduction

Due to the temporal cues present in sound signals, the auditory nervous system provides a good opportunity to explore how multiple membrane currents (intrinsic and synaptic) influence signal integration (Trussell 1999). The preservation of precise temporal information is crucial for coding and decoding, especially below about 2 kHz in mammals. Correspondingly, brainstem auditory neurons have very fast decaying synaptic currents (Raman and Trussell 1992; Gardner et al. 1999) and fast low-threshold potassium (I_{KLT}) currents (Manis and Marx 1991; Reyes et al. 1994; Rathouz and Trussell 1998). They typically fire phasically, not tonically, for step current stimuli, presumably because of I_{KLT} (Manis and Marx 1991; Reyes et al. 1994; Smith 1995; Svirskis et al. 2002). Experimental and modeling studies suggest that such biophysical properties enhance the ability of auditory neurons to synchronize (phase lock) to strong (Oertel 1983; Rothman and Young 1996;

Reyes et al. 1996) as well as to weak (Svirskis et al. 2002) sinusoidal stimuli and thus to transmit more precisely the signal's temporal information. Medial superior olivary (MSO) neurons and their avian analogs are implicated as coincidence detectors for sound localization (Jeffress 1948; Goldberg and Brown 1969; Carr and Konishi 1990) and provide an opportunity to relate membrane properties to neuronal function (Reyes et al. 1996).

A common feature of afferent input to brainstem auditory nuclei is a high level of spontaneous activity. In the absence of a sound stimulus, this random firing can reach rates of 100 Hz (Liberman 1978, 1982). Fibers with different spontaneous rate have different projections in the cochlear nucleus (Liberman 1991, 1993), suggesting a specific role of the spontaneous random activity. It is well known that noise can facilitate the detection of weak signals in diverse natural and artificial systems (Wiesenfeld and Moss 1995; Bezrukov and Vodyanoy 1995). It is possible that neuronal spontaneous activity could serve a similar function since it increases in lower auditory brainstem centers during performance (Ryan et al. 1984). Notably, some MSO cells are spontaneously active in vivo, reflecting a significant amount of random spontaneous input (Goldberg and Brown 1969; Carr and Konishi 1990; Young and Rubel 1986).

Since I_{KLT} activates below the threshold for spike generation, it is expected to play an important role in the integration of subthreshold signals. To gain more insight on this role, we studied the responsiveness of MSO neurons (gerbil, in vitro) and Hodgkin-Huxley-like models (that included currents for spike generation and I_{KLT}) to computer-generated currents that mimic transient random weak synaptic conductances. We found that blocking I_{KLT} in MSO neurons decreased the SNR when a brief subthreshold excitatory postsynaptic conductance (EPSG) "signal" was injected together with weak random excitatory and inhibitory PSGs. This input protocol also enabled us to determine, by using the reverse correlation method, the net synaptic input that leads on average to spike generation. We further saw that, in order to spike, the cell and the model with I_{KLT} selects for faster inward current transients, i.e., that its temporal integration window is narrowed. These results demonstrate benefits from I_{KLT} for detecting weak signals with increased SNR and shortening the integration time.

The neural computation for localizing low-frequency sounds involves coincidence detection of binaural inputs, as occurs in MSO. We show that a model's ITD window for spiking in response to well-timed excitatory inputs (that are individually subthreshold) narrows with increasing I_{KLT} (over a certain range). In actuality, the computation is carried out in the presence of noise and inhibition (Grothe and Sanes 1994; Brand et al. 2002). For a pure tone, say, while the auditory nerve inputs are well phase-locked (with some jitter), the probability of an auditory nerve spike per cycle is less than 1 (cycle-skipping) and decreases strongly with frequency, so stochastic factors are involved here as well. Interestingly, it was recently found in gerbils (Brand et al. 2002) that precisely timed inhibition shifts the ITD tuning curve so that it is steeply sloped around ITD = 0. Moreover, as had been seen previously (see McAlpine et al. 2001 and references therein), many ITD-sensitive cells do not have their peak locations spanning or lying within the physiological range. These results call into question (McAlpine et al. 2001) whether the classical hypothesis of a place code (Jeffress 1948) applies to small mammals even while it is widely accepted for the avian system (Carr and Konishi 1990). The model shows a similar effect from brief and time-locked inhibition, and we see that I_{KLT} contributes to the effect of inhibition on coincidence detection, at least for individually subthreshold inputs.

2 Methods

2.1 Experimental

Recordings were done at room temperature in slices from gerbils (*Meriones unguiculatus*) aged postnatal days 8–17 (P8–17) as described in (Svirskis et al. 2002). In brief, the artificial cerebrospinal fluid contained (in mM) 125 NaCl, 4 KCl, 1.2 KH_2PO_4, 1.3 $MgSO_4$, 26 $NaHCO_3$, 15 glucose, 2.4 $CaCl_2$, and 0.4 L-ascorbic acid (pH 7.3 when bubbled with 95% O_2-5% CO_2). The internal patch solution contained (in mM) 127.5 potassium gluconate, 0.6 EGTA, 10 HEPES, 2 $MgCl_2$, 5 KCl, 2 ATP, and 0.3 GTP (pH 7.2). Recording electrodes were fabricated from borosilicate glass microcapillaries (1.5 mm outer diameter), and their resistance ranged from 7 to 12 MΩ. We used the dynamic clamp method for stimulus generation (Reyes et al. 1996; Sharp et al. 1993). The program determined in real time the time-varying current that was injected into the neuron according to the calculated conductance value and the measured instantaneous membrane potential. The time course of injected current was kept in the computer memory buffer and used to calculate spike-triggered reverse correlation (Bryant and Segundo 1976; Mainen and Sejnowski 1995). Several thousand events were used for computing average spike-triggering currents and poststimulus time histograms (PSTHs). To study the integration of weak transient signals in the presence of noise, a single subthreshold "signal" synaptic conductance, EPSG, was generated as a simple exponential decay from a step onset and time constant of 1 ms. Two trains of random smaller (on average) transient EPSGs and IPSGs (1-ms decay time constants) were delivered as random trains continuously representing the "noise". For random excitation the reversal potential was 0 mV, and for inhibition it was −70 mV.

2.2 Theoretical

We used two different single-compartment (lumped neuron) models with Hodgkin-Huxley-type Na^+ and K^+ conductances for spike generation and a low-threshold potassium conductance (Brand et al. 2002; Svirskis et al. 2002; Rothman et al. 1993). For results in Figs. 1–3 the weak stimuli for the computational neuron (Svirskis et al. 2002) were the same as in experiments, except for the conductance amplitudes of the PSGs. For the simulations of coincidence detection described in Figs. 4–6 we used a different MSO model (Brand et al. 2002; Rothman et al. 1993) that incorporates similar intrinsic currents and an auditory nerve model for pure-tone input generation (Rothman et al. 1993). See the Appendix for more complete descriptions of these two models.

3 Results

3.1 I_{KLT} contributes to phasic behavior

In the majority of MSO neurons, a step stimulus would not evoke more than a single spike (Fig. 1A). Such a phasic firing pattern and the outward rectification (Fig. 1A, inset) that appears near the resting membrane potential, V_{rest}, suggest the presence of an I_{KLT} in these MSO cells. This fast and strong outward current prevented spike generation in response to slowly rising current ramps ($n = 3$), although faster ramps of the same amplitude could evoke single spikes (Fig. 1C).

The application of 10 nM dendrotoxin (DTX), which is known to block some Kv1 family potassium channel subtypes (Hopkins et al. 1994; Robertson et al. 1996), converted the phasic firing pattern of P12–14 MSO neurons into tonic firing in 9 out of 11 cases (Fig. 1B), and the cells could fire action potentials in response to slow ramps (Fig. 1D).

To confirm that the low-threshold potassium current (I_{KLT}) could account for these observed changes in response to current steps and ramps and for the integration of weak

noisy signals (see below), we carried out a modeling study. Our Hodgkin-Huxley-like model (see Methods) contains sodium and potassium currents for spike generation and a model for I_{KLT} that is based on voltage-clamp data (Rathouz and Trussell 1998). It exhibits phasic firing (Fig. 1E) and tonic firing when I_{KLT} is eliminated (Fig. 1F).

3.2 Detection of weak inputs in noise

To explore how the low-threshold outward current influenced the integration of small and random signals, we applied computer-generated dynamic clamp stimuli. For small signal detection in particular, we considered how effectively the occurrence of a subthreshold "signal" EPSG changed the firing rate in the presence of smaller random excitatory and inhibitory transients, the "noise" (Fig. 2A). For auditory neurons, this signal EPSG could represent the synchronized arrival of unitary inputs in the case of a very weak auditory stimulus.

The signal EPSG could not evoke a spike in the absence of random input. However, as seen in the computed PSTH, when the signal EPSG occurred together with noise, there was a sharp increase in firing probability over the spontaneous firing levels (Fig. 2B). To measure the efficiency of signal detection, we defined and computed the SNR as the ratio of the increased firing rate in response to the "signal" EPSG (deviation of PSTH value from its baseline) and the spontaneous firing rate in response to "noise" (Fig. 2B, inset). The application of I_{KLT} blockers lowered spike threshold and increased the spontaneous rate significantly, thus reducing the SNR ($n = 11$). That is, in the control case, I_{KLT} prevents some of the temporally summated random inputs from generating spikes while the larger-amplitude (but subthreshold) and faster signal can ride on the noise and "break through" before the transient outward rectification is fully recruited.

Our model shows these same basic response properties as MSO neurons when presented with the same (but amplitude-adjusted) stimuli as in our experiments (see Methods and Fig. 2D). The presence of I_{KLT} in the model makes the spontaneous firing rate much lower than in the model without I_{KLT} (Fig. 2E). The presence of I_{KLT} reduces the response to the signal EPSG as well, but not as much as for the spontaneous firing probability. Consequently, I_{KLT} increases the SNR (Fig. 2E, inset).

3.3 I_{KLT} narrows the temporal integration window

To observe the transient net input current that develops before an MSO neuron generates a spike, we performed a reverse correlation analysis to compute the average spike-triggering dynamic clamp "synaptic" current (Fig. 2C). As could be expected, the average spike-triggering current was predominantly an inward (depolarizing) current that developed on a time scale of 2–3 ms (Fig. 2C). The application of DTX or DTXK changed the time course of the mean spike-triggering input current: it developed more slowly (Fig. 2C). The maximal rate of mean injected current calculated for a 0.5-ms time window was significantly slower after a block of I_{KLT} ($n = 7$, $P < 0.05$ paired t-Student test) and decreased from 0.8 ± 0.38 nA/ms to 0.5 ± 0.3 nA/ms. The faster dynamics of the spike-triggering current as mediated by I_{KLT} further implicated I_{KLT}'s role in enhancing the precision of temporal processing.

For the model, the mean input current that precedes spike generation has the same shape as in MSO neurons (Fig. 2F), and it has a faster mean time course with I_{KLT} compared to when I_{KLT} is eliminated. Notice further that, in both the experimental and computational records, the mean spike-triggering current has a hyperpolarizing undershoot before its strong depolarizing rise. We interpret this hyperpolarizing "dip" as evidence of input combinations that favor spike generation by first deactivating some I_{KLT} and then providing properly

timed depolarizing input. The dip is reduced when I_{KLT} is blocked (the effect is seen more clearly in the unscaled case of Fig. 2C).

Next, we illustrate more directly the significance of I_{KLT}'s dynamic and voltage dependence specifically by comparing the model neuron's behavior as adjustments are made in the parameters of I_{KLT} that alter the activation rate τ_{KLT} of the I_{KLT} conductance or that eliminate its voltage dependence. As τ_{KLT} is decreased, the probability of firing generally decreases (Fig. 3A); the speeded up conductance acts to filter out more of the spikes coming from slower summated noisy inputs (with or without signal riding on top). But the net effect is an increase in the SNR (Fig. 3A, inset). The relative advantage of faster I_{KLT} depends on the compromise between the SNR and the strength of the response. It is tempting to view I_{KLT}'s influence as an additional conductance in the subthreshold regime that effectively shortens the membrane time constant. To examine this notion, we eliminated I_{KLT} and increased by threefold the model's leak conductance. In comparison with the control case, the SNR of these two realizations of the model were almost the same (Fig. 3B, inset); however, the response amplitude for the model with I_{KLT} was almost two times larger (Fig. 3A). Again, supposing that not only the SNR but also the strength of the response is important leads us to conclude that the subthreshold voltage-dependent outward current is important for enhancing small signal integration. Moreover, it is not adequate to view the net improvement as due only to a change in the membrane time constant.

3.4 Coincidence detection, inhibition, and subthreshold outward currents

For localizing low-frequency sounds, the detection of ITDs between binaural inputs is important (Jeffress 1948; Goldberg and Brown 1969; Carr and Konishi 1990). We address this issue here using the model in two protocols. How does I_{KLT} influence the ITD window for the neuron model to respond to two subthreshold inputs or to, in a more in vivo-like caricature, an ensemble of periodically Poisson-modulated input trains as might be delivered from phase-locked but cycle-skipping firings of auditory nerve fibers from ipsilateral and contralateral sides? In each case, motivated by recent in vivo experimental and computational findings (Brand et al. 2002), we allow for the effects of brief transient inhibitory inputs that might be time locked to excitatory inputs (from the contralateral side). We adopt the same model as was used in (Brand et al. 2002) (see Methods).

When two identical but individually subthreshold inputs are presented to the noise-free model, a spike is elicited if the inputs occur within a critical ITD window around perfect coincidence (provided, of course, that a doubled-amplitude input is superthreshold) (Fig. 4A). As one expects, this window for detection of the pair narrows as I_{KLT} is strengthened (by increasing G_{KLT}), i.e., timing selectivity is enhanced (Fig. 4B). But again one sees that there is a compromise between this enhanced temporal filtering and signal throughput. If G_{KLT} is made too large, the cell cannot respond to even a perfectly coincidental presentation of inputs at this amplitude. In Figs. 4–6, ITD < 0 corresponds to the "ipsilateral" input leading.

The effect of a brief inhibitory input that is time locked to just precede (by 0.4 ms) the contralateral input is to narrow the ITD window for detection (Fig. 4A, dashed). The ipsilateral leading side is affected more, i.e., when the inhibitory input occurs between the two excitatory inputs. The conditions for firing are disfavored if the preceding excitatory input has created a larger transient of I_{KLT} (or, more accurately, of I_{KLT}'s conductance). This occurs here when the ipsilateral excitatory (full strength) input precedes the composite input, the combination of contralateral inhibition followed shortly by the contralateral excitation.

When multiple ipsilateral and contralateral input lines are incorporated into the model (see Methods and Appendix) with stochastic but phase-locked EPSG events that idealize auditory nerve responses, ITD tuning to a pure tone is seen (Fig. 5A). Here the sculpting out of the ITD window on the ipsilateral-leading side with increasing inhibition (as in Fig. 4A) is also apparent. The effective rightward shift, with the tuning curve's peak not at ITD = 0, is presented (Brand et al. 2002) as evidence of inhibition's involvement in the hypothesis that the coding of sound localization may not involve the location of the peak (as in the classical Jeffress model (Jeffress 1948)) but rather involves the region around ITD = 0 where the response is most sensitive to ITD variation – i.e., a slope code rather than a place code. This relates to our general notion (as above in Fig. 4) that subthreshold outward currents (in this case, also synaptic) can influence temporal processing in MSO neurons. However, our main points in this paper are the effects of I_{KLT}, not I_{syn}, on tuning and temporal processing.

As G_{KLT} is increased, we see that the firing rate decreases at all ITDs shown here – and irrespective of whether inhibition is included (Fig. 5B). Both the peaks and the troughs of the tuning curves are considerably affected. To compare the shape changes in these curves and possibly detect some relative narrowing as G_{KLT} is increased, we first rescale the curves (divide the ordinate values by the mean of the peak and trough rates) to bring them into the same response range (Fig. 6A). In this representation, it seems to the naked eye as though increasing G_{KLT} leads to a steeper sloped tuning curve between the peak and trough – sharper tuning. By defining a shape index parameter as the difference between the peak and trough in this scaled representation we see that tuning sharpens (shape index increases) as G_{KLT} is increased (Fig. 6B, left). On the other hand, the response decreases (Fig. 6B, right) – meaning again a tradeoff between enhancement of coincidence detection and signal throughput. The shape index curves are affected somewhat by inhibition, but these curves do not reveal the inhibition-induced rightward shift (which is actually reduced slightly for increasing G_{KLT}, not shown). In contrast to our considerations in previous sections of how I_{KLT} affects the integration of weak signals in noise, here the signals are not weak and I_{KLT} acts, through its conductance, more via a shunting mechanism than through a dynamic selective filtering mechanism.

4 Discussion

Low-threshold potassium currents enhance temporal processing and sensitivity to spike timing in the auditory system, and we have seen these effects in several ways. In gerbil MSO neurons, the DTX-sensitive I_{KLT} increased the SNR for a *subthreshold* signal in the presence of weak random input. A computational model with Hodgkin-Huxley-type conductances for spike generation and I_{KLT} had the same qualitative integration properties for noisy signals as did MSO neurons in vitro. By using the reverse correlation method we can see that I_{KLT} shortens the integration time window for the neurons and the model. Both the voltage and time dependence of the subthreshold outward current contribute to enhancing weak signal integration. If I_{KLT} activates more rapidly, the phasic filtering properties are enhanced but at some cost of lower throughput. If it is too slow, then G_{KLT} acts to effectively increase the leakage conductance. The resulting SNR could match that of the model with I_{KLT}, but the response to the signal is significantly reduced; the benefits of dynamic voltage-gated filtering are not realized. Increasing the strength of I_{KLT} tightens the model's critical temporal window for coincidence detection of weak signals. For stronger signals, I_{KLT}'s effect is more like a shunt and perhaps less selective. Again, the enhancements must be weighed against reduction of overall response. Brief inhibition contributes to shaping the ITD tuning curve.

The ability of neuronal properties to influence signal integration in the presence of noise was extensively investigated previously. For example, such studies suggested that an interaction

between noisy signals and voltage-dependent currents could bring about increased temporal precision (Gauck and Jaeger 2000), improved coincidence detection (Softky and Koch 1993; Softky 1994), increased information transfer (Manwani and Koch 1999), and spike-timing reliability (Mainen and Sejnowski 1995; Hunter et al. 1998). Our studies concentrated on the effects of a particular current, I_{KLT}, and tried to elucidate the mechanisms by which neurons could improve small or strong signal integration.

In a separate computational study (Svirskis and Rinzel 2003), we have shown that an integrate-and-fire-type model without an I_{KLT} but with an idealized sub-threshold inward current can behave phasically if the inward current inactivates with an appropriate time scale and in a voltage range below its activation threshold; the model also shows improved SNR as compared with the case with no subthreshold inactivation. Thus, multiple forms of subthreshold fast, but not necessarily instantaneous, negative feedback can contribute to enhancing temporal processing.

We have emphasized that the dynamic aspects (i.e., the time scale of the gating kinetics) of I_{KLT} activation are important for understanding how I_{KLT} affects signal throughput (Fig. 3). Fast just-suprathreshold depolarizing inputs can squeeze through to spike threshold before I_{KLT} is activated, while slower ones that would be suprathreshold, if the membrane conductance remained at its resting level, will now be rendered subthreshold because there will be adequate time for reducing the membrane resistance by activating the conductance of I_{KLT}. In this sense, I_{KLT} effectively acts to implement a dynamic threshold or filter. Here we have considered a spontaneous state of noisy fast weak inputs. A few nearly coincident ones provide fast depolarization that can lead to a spontaneous firing. Occasionally, some of these, not so nearly coincident, will summate temporally to create a slower transient that would be suprathreshold if it were not falling into the temporal window for recruiting I_{KLT}. Therefore, I_{KLT} can eliminate false positives.

We have shown with a model that detection of nearly coincident "binaural" inputs is improved by I_{KLT}. For subthreshold inputs, I_{KLT} exerts its dynamic filtering property (Fig. 4). It also interacts with brief inhibition (timed to just precede contralateral excitation) to shape the ITD tuning properties, narrowing and shifting the tuning range's center toward the contralateral-leading direction (Fig. 4, dashed). For strong inputs, I_{KLT} acts more like a shunt lowering the overall firing rates while sharpening ITD tuning (Fig. 6). Inhibition shifts the peak of the ITD tuning curve, suggesting a slope code ((Brand et al. 2002), and Figs. 4–6 here). A better understanding of I_{KLT}'s effect on the inhibition-induced reshaping and shifting in the strong input case (Fig. 6b) will be sought in future studies.

Various investigators have proposed that low-threshold potassium currents help to suppress weak subthreshold inputs while improving the temporal precision of integration of strong suprathreshold inputs (Brew and Forsythe 1995; Oertel 1983; Manis and Marx 1991; Rathouz and Trussell 1998; Reyes et al. 1994; Rothman and Young 1996). It is important to stress that, in the case of weak subthreshold inputs, the noise is necessary so that the neuron can detect a potentially meaningful subthreshold signal. On the other hand, if the signal is absent, noise creates false positives. The low-threshold potassium current in such circumstances plays two roles: it allows the noise to aid in signal detection, while it suppresses false positives if the signal is absent.

Acknowledgments

References

Bezrukov SM, Vodyanoy I. Noise-induced enhancement of signal transduction across voltage-dependent ion channels. Nature. 1995; 378:362–364. [PubMed: 7477370]

Brand A, Behrend O, Marquardt T, McAlpine D, Grothe B. Precise inhibition is essential for microsecond interaural time difference coding. Nature. 2002; 417:543–547. [PubMed: 12037566]

Brew HM, Forsythe ID. Two voltage-dependent K$^+$ conductances with complementary functions in postsynaptic integration at a central auditory synapse. J Neurosci. 1995; 15:8011–8022. [PubMed: 8613738]

Bryant HL, Segundo JP. Spike initiation by transmembrane current: a white-noise analysis. J Physiol. 1976; 260:279–314. [PubMed: 978519]

Carr CE, Konishi M. A circuit for detection of interaural time differences in the brain stem of the barn owl. J Neurosci. 1990; 10:3227–3246. [PubMed: 2213141]

Gardner SM, Trussell LO, Oertel D. Time course and permeation of synaptic ampa receptors in cochlear nuclear neurons correlate with input. J Neurosci. 1999; 19:8721–8729. [PubMed: 10516291]

Gauck V, Jaeger D. The control of rate and timing of spikes in the deep cerebellar nuclei by inhibition. J Neurosci. 2000; 20:3006–3016. [PubMed: 10751453]

Goldberg JM, Brown PB. Response of binaural neurons of dog superior olivary complex to dichotic tonal stimuli: some physiological mechanisms of sound localization. J Neurophysiol. 1969; 32:613–636. [PubMed: 5810617]

Grothe B, Sanes DH. Synaptic inhibition influences the temporal coding properties of medial superior olivary neurons: an in vitro study. J Neurosci. 1994; 14:1701–1709. [PubMed: 8126564]

Hopkins WF, Allen ML, Houamed KM, Tempel BL. Properties of voltage-gated K$^+$ currents expressed in Xenopus oocytes by mKv1.1, mKv1.2 and their heteromultimers as revealed by mutagenesis of the dendrotoxin-binding site in mKv1.1. Pflugers Arch. 1994; 428:382–390. [PubMed: 7816560]

Hunter JD, Milton JG, Thomas PJ, Cowan JD. Resonance effect for neural spike time reliability. J Neurophysiol. 1998; 80:1427–1438. [PubMed: 9744950]

Jeffress LA. A place theory of sound localization. J Comp Physiol Psychiatry. 1948; 41:35–39.

Liberman MC. Auditory-nerve response from cats raised in a low-noise chamber. J Acoust Soc Am. 1978; 63:442–455. [PubMed: 670542]

Liberman MC. Single-neuron labeling in the cat auditory nerve. Science. 1982; 216:1239–1241. [PubMed: 7079757]

Liberman MC. Central projections of auditory-nerve fibers of differing spontaneous rate. I. Anteroventral cochlear nucleus. J Comp Neurol. 1991; 313:240–258. [PubMed: 1722487]

Liberman MC. Central projections of auditory nerve fibers of differing spontaneous rate. II. Posteroventral and dorsal cochlear nuclei. J Comp Neurol. 1993; 327:17–36. [PubMed: 8432906]

Mainen ZF, Sejnowski TJ. Reliability of spike timing in neocortical neurons. Science. 1995; 268:1503–1507. [PubMed: 7770778]

Manis PB, Marx SO. Outward currents in isolated ventral cochlear nucleus neurons. J Neurosci. 1991; 11:2865–2880. [PubMed: 1880553]

Manwani A, Koch C. Detecting and estimating signals in noisy cable structures. II. Information theoretical analysis. Neural Comput. 1999; 11:1831–1873. [PubMed: 10578034]

McAlpine D, Jiang D, Palmer AR. A neural code for low-frequency sound localization in mammals. Nat Neurosci. 2001; 4:396–401. [PubMed: 11276230]

Oertel D. Synaptic responses and electrical properties of cells in brain slices of the mouse anteroventral cochlear nucleus. J Neurosci. 1983; 3:2043–2053. [PubMed: 6619923]

Raman IM, Trussell LO. The kinetics of the response to glutamate and kainate in neurons of the avian cochlear nucleus. Neuron. 1992; 9:173–186. [PubMed: 1352983]

Rathouz M, Trussell LO. Characterization of outward currents in neurons of the avian nucleus magnocellularis. J Neurophysiol. 1998; 80:2824–2835. [PubMed: 9862887]

Reyes A, Rubel EW, Spain WJ. Membrane properties underlying the firing of neurons in the avian cochlear nucleus. J Neurosci. 1994; 14:5352–5364. [PubMed: 8083740]

Reyes A, Rubel EW, Spain WJ. In vitro analysis of optimal stimuli for phase-locking and time-delayed modulation of firing in avian nucleus laminaris neuron. J Neurosci. 1996; 16:993–1007. [PubMed: 8558268]

Robertson B, Owen D, Stow J, Butler C, Newland C. Novel effects of dendrotoxin homologues on subtypes of mammalian Kv1 potassium channels expressed in Xenopus oocytes. FEBS Lett. 1996; 383:26–30. [PubMed: 8612784]

Rothman JS, Young ED. Enhancement of neural synchronization in computational models of ventral cochlear nucleus bushy cells. Audit Neurosci. 1996; 2:47–62.

Rothman JS, Young ED, Manis PB. Convergence of auditory nerve fibers onto bushy cells in the ventral cochlear nucleus: implications of a compartmental model. J Neurophysiol. 1993; 70:2562–2583. [PubMed: 8120599]

Ryan AF, Miller JM, Pfingst BE, Martin GK. Effects of reaction time performance on single-unit activity in the central auditory pathway of the rhesus macaque. J Neurosci. 1984; 4:298–308. [PubMed: 6693945]

Sharp AA, O'Neil MB, Abbott LF, Marder E. The dynamic clamp: artificial conductances in biological neurons. Trends Neurosci. 1993; 16:389–394. [PubMed: 7504352]

Smith PH. Structural and functional differences distinguish principal from nonprincipal cells in the guinea pig mso slice. J Neurophysiol. 1995; 73:1653–1667. [PubMed: 7643173]

Softky W. Sub-millisecond coincidence detection in active dendritic trees. Neuroscience. 1994; 58:13–41. [PubMed: 8159289]

Softky W, Koch C. The highly irregular firing of cortical cells is inconsistent with temporal integration of random EPSPs. J Neurosci. 1993; 13:334–350. [PubMed: 8423479]

Svirskis G, Rinzel J. Influence of subthreshold nonlinearities on signal-to-noise ratio and timing precision for small signals in neurons: minimal model analysis. Netw Comput Neural Sys. 2003; 14:137–150.

Svirskis G, Kotak V, Sanes DH, Rinzel J. Enhancement of signal-to-noise ratio and phase locking for small signals by a low threshold outward current in auditory neurons. J Neurosci. 2002; 22:11019–11025. [PubMed: 12486197]

Trussell LO. Synaptic mechanisms for coding timing in auditory neurons. Annu Rev Physiol. 1999; 61:477–496. [PubMed: 10099698]

Wiesenfeld K, Moss F. Stochastic resonance and the benefits of noise: from ice ages to crayfish and squids. Nature. 1995; 373:33–36. [PubMed: 7800036]

Young SR, Rubel EW. Embryogenesis of arborization pattern and topography of individual axons in n. laminaris of the chicken brain stem. J Comp Neurol. 1986; 254:425–459. [PubMed: 3805357]

Appendix A: Model used for Figs. 1–3

The currents were calculated by using the general equation $I = gA_{cell}m^p h^q (V - E)$, where g is specific conductance, A_{cell} is membrane area, p and q represent the numbers of gating subunits, V is membrane potential, and E is reversal potential for the current. Activation and inactivation gating variables, m and h respectively, were governed by equations of the form $du/dt = (u_\infty - u)/\tau_u$. The "steady state" value for the gating variable, u, was $u_\infty = \alpha/(\alpha + \beta)$ and time constant $\tau_u = 1/(\alpha + \beta)$; both u_∞ and τ_u were voltage dependent: $\alpha = A_0 \exp\{-0.0393z\gamma(V_{0.5} - V)\}$, $\beta = B_0 \exp\{0.0393z(1 - \gamma)(V_{0.5} - V)\}$, where z is the effective gating charge. The fast-activating sodium current had a reversal potential of $E = 50$ mV; its activation was described by the parameters $p = 3$, $z = 3.3$, $\gamma = 0.7$, $A_0 = 4.2$ ms^{-1}, $B_0 = 4.2$ ms^{-1}, $V_{0.5} = -29.5$ mV; inactivation had the following parameters: $q = 1$, $z = -3.0$, $\gamma = 0.27$, $A_0 = 0.09$ ms^{-1}, $B_0 = 0.09$ ms^{-1}, $V_{0.5} = -40$ mV. The time constants for activation and inactivation had limits to their minimal values set to 0.05 and 0.25 ms, respectively, to avoid exponents from occasional overflowing. The delayed rectifier conductance had only an activation gating variable, described by the parameters: $E = -90$ mV, $p = 4$, $z = 3$, $\gamma =$

0.8, $A_0 = 0.3$ ms^{-1}, $B_0 = 0.3$ ms^{-1}, $V_{0.5} = -30$ mV, and the minimal time constant for activation of 1 ms. The conductance of the low-threshold potassium current, I_{KLT}, was described by the parameters: $E = -90$ mV, $p = 1$, $z = 2.88$, $\gamma = 0.39$, $A_0 = 0.2$ ms^{-1}, $B_0 = 0.17$ ms^{-1}, $V_{0.5} = -45$ mV. This current did not inactivate.

The specific conductances, g, were 0.1 nS/μm^2, 0.01 nS/μm^2, and 0.005 nS/μm^2 for Na^+, K^+, and I_{KLT} conductances, respectively. The area of the compartment, A_{cell}, was 104 μm^2; specific conductance for membrane leakage was 3.333×10^{-3} nS/μm^2; specific capacitance was 10^{-5} nF/μm^2 with the resulting time constant τ_m of 3 ms. The model's rest potential was about -60 mV, and the spike threshold was about 20 mV above rest.

Appendix B: Model used for Figs. 4–6

A single-compartment model described by Hodgkin-Huxley-type equations that incorporate Na^+, K^+, and low-threshold potassium conductances is used. The model is identical to the one used earlier in modeling bushy cells of antroventral cochlear nucleus by Roth-man et al. (Rothman and Young 1996), as well as simulating MSO neurons to study ITD shifts caused by contralateral inhibition (Brand et al. 2002). Our parameters, voltage dependences of the rate constants and a Poisson spike generation mechanism including the refractory function, are the same as those of Rothman et al. In simulating 2×25 excitatory and 25 inhibitory inputs the parameters we used for Poisson spike generation are $R_{ss} = 90$, $R_r = R_{st} = 0$. The membrane evolution equation is $C_{tot} dV/dt = -G_L(V - E_L) - G_{Na} m^2 h(V - E_{Na}) - G_K n(V - E_K) - G_{KLT} w(V - E_K) - G_e(V - E_E) - G_i(V - E_I)$. The membrane conductance is $C_{tot} = 23$ pF. The activation variables m, n, and w and the inactivation variable h evolve according to $d\eta/dt = a_\eta(1 - \eta) - \beta_\eta \eta$, for $\eta = m, n, w$, and h. The voltage dependences of a_η and β_η are identical to those listed in the Appendix of Rothman et al. (Rothman et al. 1993) at temperature $T = 38$°C. The absolute conductance values are $G_L = 5.2$ nS, $G_{Na} = 985.2$ nS, $G_K = 173.3$ nS. The reversal potentials are $E_{Na} = 55$ mV, $E_L = 2.8$ mV, $E_K = -77$ mV, $E_E = -10$ mV, $E_I = -66.5$ mV. The value of G_{KLT} is fixed at 86.6 nS for Fig. 5A but varied for other figures as indicated in the figure captions. The time constants of excitation and inhibition for Fig. 4 are 0.3 ms for each but 0.1 ms for Fig. 5 and Fig. 6. Figure 4 uses single deterministic alpha-function synapses. Figures 5 and 6 use 2×25 excitatory and 25 inhibitory presynaptic inputs given as alpha functions generated at intervals specified by independent Poisson spike trains whose rate is modulated with a stimulus frequency of 500 Hz. The inhibitory synapses precede the contralateral excitation by 0.2 ms as in Brand et al. (Brand et al. 2002).
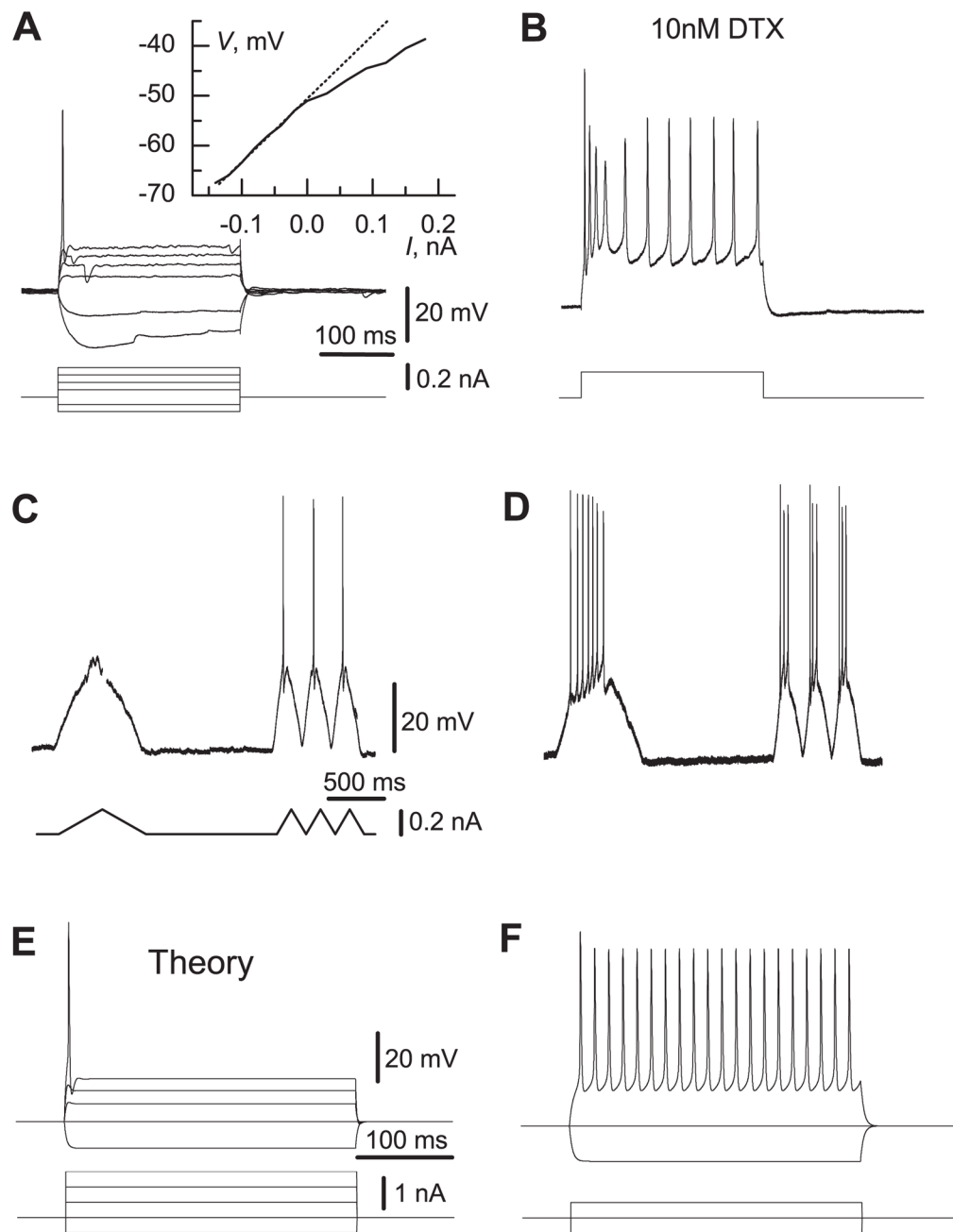
Fig. 1.
Fig. 1A–F. The firing properties of MSO neurons and models. **A** In response to a step current injection, MSO neurons showed outward rectification and only a single spike when the stimulus exceeded the threshold (phasic firing). The steady state current–voltage curve (*inset*) generated from the responses to step current stimuli showed that low-threshold outward rectification appeared near the resting membrane potential. The same properties suppressed firing in response to a slow triangular current ramp stimulus while faster stimuli evoked single spikes (**C**). **B** After an application of DTX the cells fired tonically and responded with spikes to a slow current ramp stimulus (**D**). **E** The model neuron showed similar response and firing properties. **F** The model without I_{KLT} responded with tonic firing

to the current injection, which was three times weaker. The scales in **B**, **D**, and **F** are the same as in **A**, **C**, and **E**, respectively. **A** and **B** are from the same P14 neuron. **C** and **D** are from the same P12 neuron
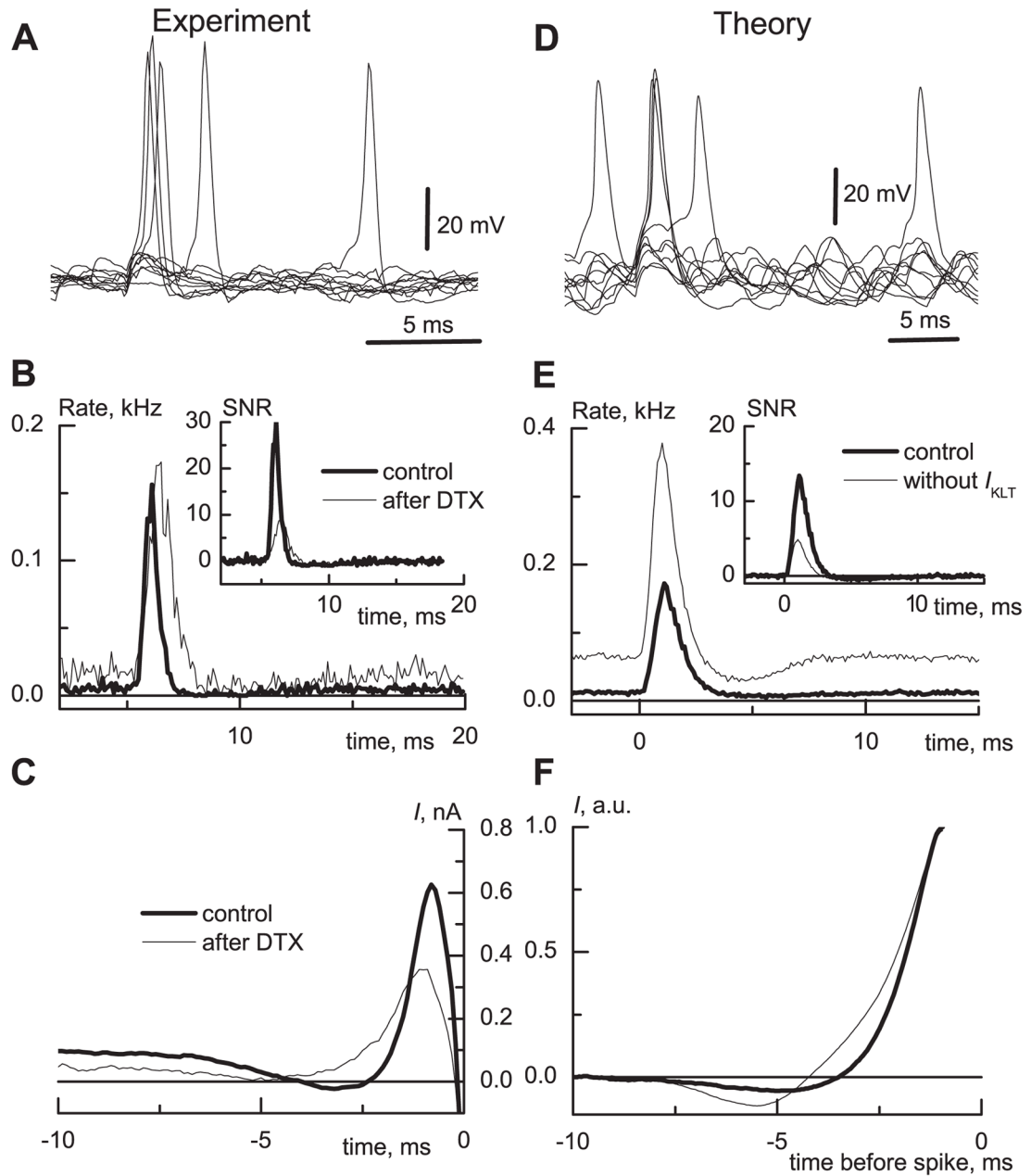
Fig. 2.

Fig. 2A–F. The firing statistics of MSO neuron and model in response to weak and noisy stimuli. **A** Traces of membrane potential illustrating random and "signal"-evoked firing. **B** The PSTH for the response to a subthreshold EPSP "signal" in the presence of smaller random excitatory and inhibitory input transients. The EPSG, generated by dynamic clamp, in addition to the random input caused a sharp increase in the probability to fire. DTX increased the spontaneous firing rate and thereby reduced the signal-to-noise ratio (SNR) several times (*inset* labeled SNR shows difference of PSTH probability from baseline, then divided by baseline). **C** A spike-triggered reverse correlation exhibited a hyperpolarizing component followed by excitation in control conditions. In the presence of DTX, an average spike-evoking current developed slower. The baselines were not subtracted. **D** Traces of

membrane potential of a model with Hodgkin-Huxley type conductances. **E** The PSTH for a subthreshold EPSP in the presence of random input. The low-threshold outward current reduced the spontaneous firing rate to 2 Hz but increased the SNR (*inset*). **F** The spike-triggered reverse correlation had the same shape as for the recorded neurons, with a hyperpolarizing component and faster dynamics for the spike-evoking current in the model with I_{KLT}. The traces were normalized and baselines subtracted to compare the time course shapes more easily
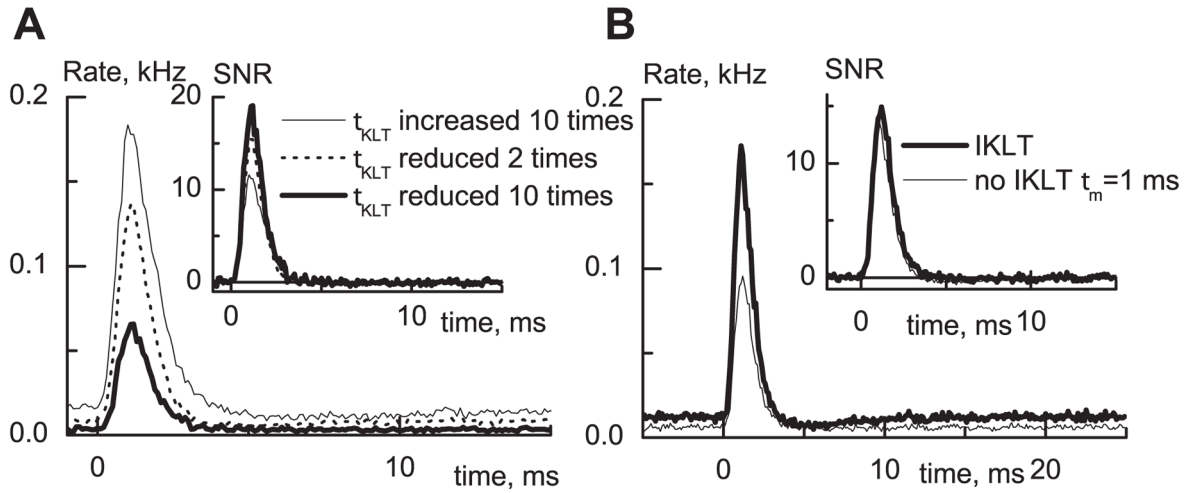
Fig. 3.
Fig. 3A,B. Influence of I_{KLT} properties on small signal integration in the model. **A** Very slow I_{KLT} activation increases spontaneous activity, while very fast activation strongly suppresses both the response to the signal and spontaneous activity. Parameters A_0 and B_0 were changed to speed up or slow down the activation of I_{KLT}. **B** When I_{KLT} is replaced by an increased leak conductance in the model, the SNR is little changed, although suppression of the response was stronger without I_{KLT}
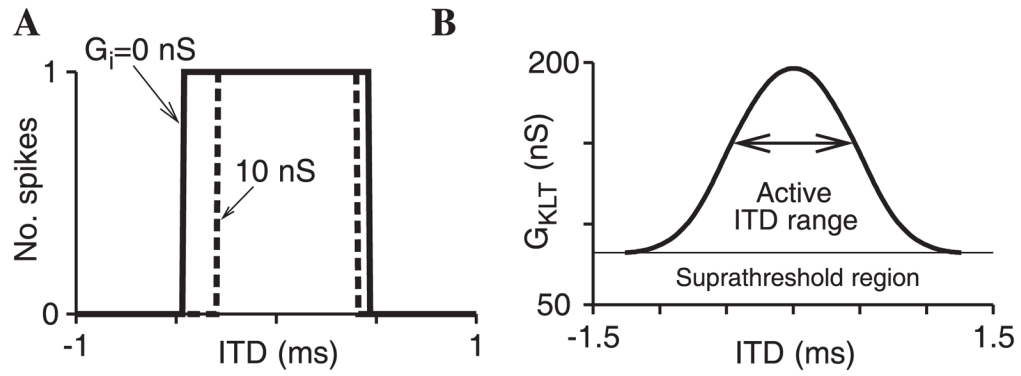
Fig. 4.
Fig. 4A,B. Effect of inhibition and I_{KLT} on coincidence detection for individual input pairs. **A** Response vs. ITD for single subthreshold contralateral and ipsilateral excitatory synaptic events, with $G_e = 8.2$ nS and contralateral inhibition that leads the contralataral excitation by 0.4 ms at $G_{KLT} = 150$ nS. The *solid curve* is for $G_i = 0$ nS, and the *dashed curve* is for 10 nS. Positive ITD indicates contralateral leading. The response range is depressed more on the ipsileading side than on the contraleading side. **B** The subthreshold contra- and ipsilateral synapses with $G_e = 8.2$ nS evoke a spike for a range of ITD values. This ITD window is shown as a function of G_{KLT}; $G_i = 0$; the *arrow* corresponds to the ITD curve shown in **A**. For smaller values of G_{KLT}, a single synapse would itself evoke action potential exhibiting suprathreshold behaviour
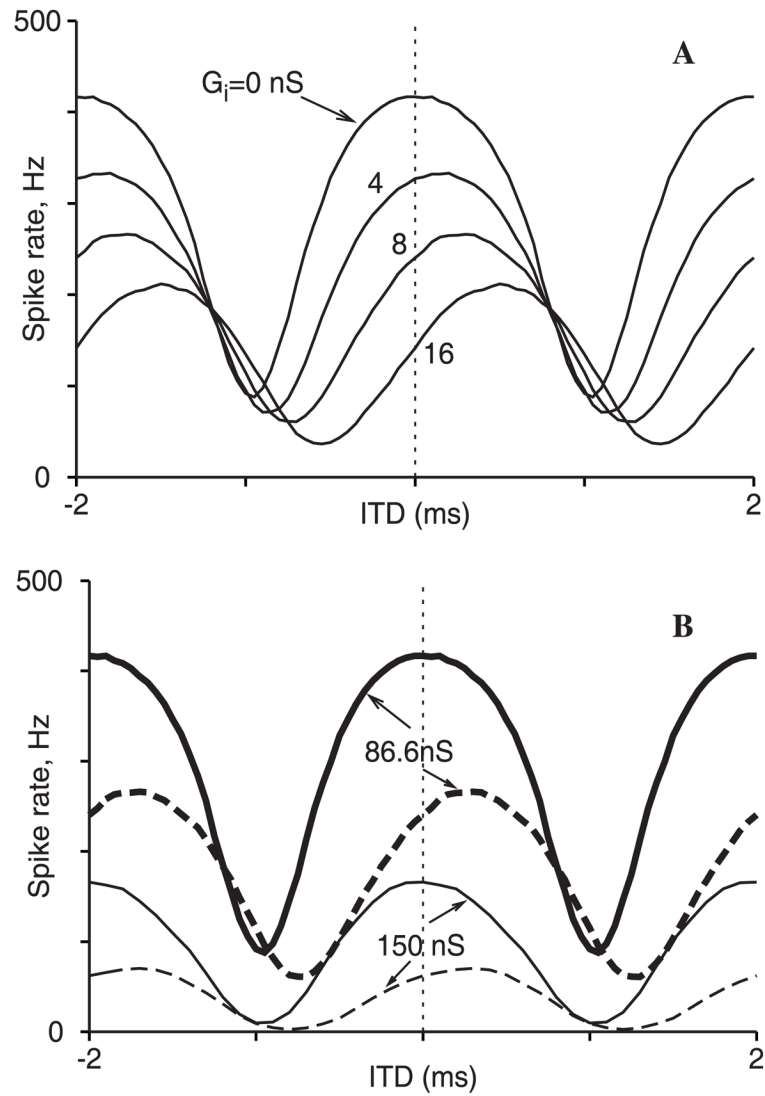
Fig. 5.
Fig. 5A,B. Dependence of ITD tuning curves on brief inhibition and I_{KLT}. (See Appendix for model description.) Maximum excitatory synaptic strength is 3 nS, and stimulus frequency is 500 Hz. **A** ITD responses as the maximum inhibitory synaptic strength is increased from 0 to 16 nS. **B** Effect of G_{KLT} on ITD tuning properties, shown for two values of G_i: 0 nS (*solid*) and 8 nS (*dashed*) as in **A**. The *thick* and *thin curves* are, respectively, for G_{KLT} = 86.6 nS and 150 nS. Increasing G_{KLT} reduces the response at each ITD and level of inhibition
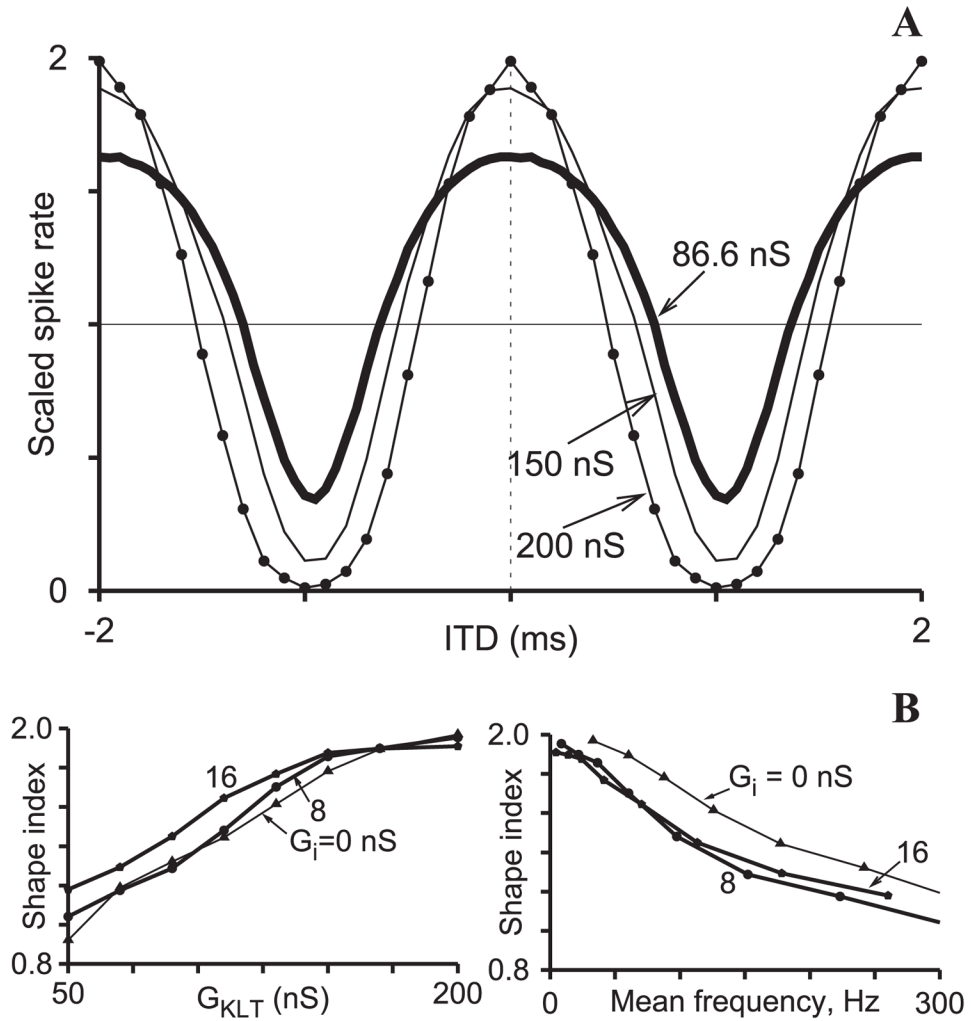
Fig. 6.

Fig. 6A,B. Dependence of ITD tuning sensitivity on I_{KLT}; $G_e = 3$ nS. **A** Effect of G_{KLT} on ITD curves (with $G_i = 0$) shown for three values of G_{KLT}: 86.6 nS (thick solid curve), 150 nS (thin curve), and 200 nS (thin curve with dots). Each curve is scaled by dividing spiking rate by the average of maximum and minimum responses for that curve. **B** Shape index, defined as the ratio of the difference and the mean of the maximum and minimum of the ITD response curves, shown as a function of G_{KLT} (left). As G_{KLT} increases, the ITD sensitivity (shape index) increases, but the corresponding response frequency (mean of maximum and minimum on a tuning curve) decreases (right). Curves are plotted for three values of $G_i = 0$, 8, and 16 nS